

Supporting Information

Transforming Metal-Organic Frameworks into Porous Liquids via a Covalent Linkage Strategy for CO₂ Capture

Dechao Wang,[†] Yangyang Xin,[†] Xiaoqian Li,[†] Hailong Ning,[‡] Yudeng Wang,[†] Dongdong Yao,^{*,†} Yaping Zheng,^{*,†} Zhuoyue Meng,[‡] Zhiyuan Yang,^{*,‡,§} Yuting Pan,[◇] Peipei Li,[⊥] Hongni Wang,[†] Zhongjie He,[†] and Wendi Fan[†]

[†] School of Chemistry and Chemical Engineering, Northwestern Polytechnical University, Xi'an 710129, P.R. China

[‡] College of Chemistry and Chemical Engineering, Xi'an University of Science and Technology, Xi'an 710021, P.R. China

[§] Key Laboratory of Coal Resources Exploration and Comprehensive Utilization, Ministry of Natural Resources, Xi'an 710021, P.R. China

[◇] Queen Mary University of London Engineering School, Northwestern Polytechnical University, Xi'an 710129, Shaanxi, P.R. China

[⊥] School of Advanced Materials and Nanotechnology, Xidian University, Xi'an, Shaanxi, 710071, P.R. China

*Corresponding authors. *E-mail addresses: yaodd@nwpu.edu.cn (D.D. Yao), zhengyp@nwpu.edu.cn (Y.P. Zheng), zhiyuanyang@126.com (Z.Y. Yang)

TABLE OF CONTENTS

1. EXPERIMENTAL SECTION

1.1 Synthesis of ZIF-8

1.2 Synthesis of ZIF-8-NH₂

1.3 Preparation of ZIF-8-NH₂ PLs

1.4 Gas breakthrough experiments

2. MOLECULAR SIMULATIONS

2.1 Molecular Models Construction

2.2 Force Fields

2.3 Simulation and Analysis Details

3. DATA ANALYSIS

Fig. S1. Synthesis of oligomer species of KH560-M2070.

Fig. S2. Synthesis of UiO-66-liquid and the illustration of surface changes of UiO-66-OH.

Fig. S3. Synthesis of oligomer species of (a) KH560-M1000 and (b) KH560-T5000.

Figure S4. The synthesis of ZIF-8-NH₂ PLs.

Figure S5. Schematic diagram of installation for breakthrough curve experiments.

Figure S6. The actual pictures of breakthrough curve experiments, (a) The operation panel; (b)

The on-line CO₂ detector; (c) Real time control and displaying module.

Figure S7. Schematic representation of the breakthrough column loading with PLs.

Figure S8. TEM images of UiO-66-OH (a, b, c) and UiO-66-liquid (d, e, f), respectively.

Figure S9. SEM images of UiO-66-OH (a, b, c) and UiO-66-liquid (d, e, f), respectively.

Figure S10. EDS mapping (C, N, Zr) of (a) UiO-66-OH and (b) UiO-66-liquid, respectively.

Figure S11.. Photos of the pristine UiO-66-OH (a₁) and UiO-66-liquid (b₁) in various common solvents at a concentration of 20 mg·mL⁻¹ as well as after setting for one week (a₂, b₂). The solvents in every photos from left to right are as following: ethanol, DMF, pyridine, chloroform, acetone and tetrahydrofuran (THF).

Figure S12. Photos of UiO-66-liquid and the fluidity of UiO-66-liquid after setting for eight months at room temperature.

Figure S13. Photos of UiO-66-liquid-M1000.

Figure S14. The photo of UiO-66-liquid-T5000.

Figure S15. TEM images of ZIF-8-NH₂ (a, b) and ZIF-8-NH₂ PLs (c, d).

Figure S16. Photos of ZIF-8-NH₂ PLs.

Figure S17. CO₂ adsorption-desorption isotherms of UiO-66-liquid under high pressure (0~30000 mbar) at 25°C. Closed and open symbols represent to adsorption and desorption, respectively.

Figure S18. CO₂ adsorption-desorption isotherms of UiO-66-liquid-M1000 under low testing pressure (0~10000 mbar) at 25 °C. Closed and open symbols represent to adsorption and desorption, respectively.

Figure S19. N₂ adsorption isotherms of UiO-66-liquid-M1000 under low testing pressure (0~10000 mbar) at 25°C.

1. EXPERIMENTAL SECTION

1.1 Synthesis of ZIF-8

ZIF-8 was prepared according to previous report with some modifications.^{1,2} In a typical procedure, ZIF-8 was synthesized by mixing two separate solutions of zinc acetate dehydrate (0.3 g) (Solution A) and 2-methylimidazole (mim, 1.56 g with 2.0 mg CTAB) (Solution B), which are dissolved in 5 mL DI water, respectively. The reaction was carried out by rapidly pouring mim Solution B into Solution A with stirring for 15 s, followed by setting for 2 h at room temperature. The ZIF-8 white precipitates were acquired by centrifugation and rinsed with MeOH. These purification steps were repeated 3 times. The obtained ZIF-8 resultants were stored in MeOH for future use.

1.2 Synthesis of ZIF-8-NH₂

A post-synthetic modification (PSM) method was used for the synthesis of ZIF-8-NH₂.³ The ZIF-8 (0.2 g) was firstly well dispersed in 100 mL MeOH. Then, Atz (0.585 g) was added to the ZIF-8 suspension. The PSM reaction was performed at room temperature for 15 min. For purification, we repeated centrifugation and rinsing steps three times with toluene. The obtained ZIF-8-NH₂ resultants were stored in toluene for future use.

1.3 Preparation of ZIF-8-NH₂ PLs

To begin with, ZIF-8-NH₂ (0.2 g) was dispersed in 20 mL toluene solution and sonicated for 10 min. Then, PDMS-epoxy (2.0 g) was added to the ZIF-8-NH₂ suspension under stirring at 100°C for 5 h to form a stable solution. The resulting solution was dried on a hot plate at 80°C and was kept at 80°C under vacuum to get ZIF-8-NH₂ PLs for use.

1.4 Gas Breakthrough Experiments

The apparatus of breakthrough testing was shown in Figure S1 and Figure S2. In the separation experiments, samples (ca. 2.0 g) were added into a special testing cavity for PLs (Figure S3), in which He used as carrier gas to flush the adsorption bed for more than 30 min as pretreatment prior to each test. Then the mixture gas flow ($\text{CO}_2/\text{N}_2=15/85$ Vol%) at a rate of $100 \text{ mL}\cdot\text{min}^{-1}$ was continuously passed through the testing cavity. The obtained data were collected and analyzed via a on-line CO_2 detector (Figure S2), which is a high-precision infrared CO_2 concentration detector (PN-2000- CO_2 -IR). Meanwhile, the real-time changes of CO_2 concentration was collected by a computer and shown on the screen.

2. MOLECULAR SIMULATION

The molecular simulation was performed using Material Studio (7.0) package (*Accelrys Software Inc*). The purpose is to verify the permanent porosity in UiO-66-liquid *via* analyzing Fractional accessible volume (FAV) and the gas adsorption density filed distribution by Grand Canonical Monte Carlo (GCMC) simulation. ⁴

2.1 Molecular Models Construction

In the beginning, molecular models of oligomer species, UiO-66-OH and UiO-66-liquid were constructed using *Amorphous Cell module*. Then, the constructed UiO-66-liquid were subjected to geometry optimization and following structural relaxation *via* annealing process. Finally, the obtained low-energy configurations were further optimized by 500-ps NVT molecular dynamics (MD) and 200-ps NPT MD to monitor the fluctuation of density. Afterward, the obtained optimum structure was used to construct models in the following procedures.

Next, the UiO-66-liquid model was constructed using *Amorphous Cell* module. All these cells with cubic form were built with 5 output frames and the initial density was set on 0.2 g/cm³ at 298 K.⁵ Then, all of amorphous cells were optimized *via* geometry optimization. The local energy was minimized by the smart minimizer method. During the minimization, the convergence level was set to 0.001 kcal/mol/Å. Subsequently, the obtained lowest energy configurations were all subjected to annealing process, in which temperature was increased from 298 K to 600 K. The highest temperature was well above the glass transition temperature (T_g) of oligomer species. And then it was cooled back at intervals of 5 K at each step in which 200 ps-NVT dynamics was carried out. Thereafter, a 500-ps MD simulation in an NVT ensemble was done to relax the structure, in which time step was 1 fs and Nose thermostat were utilized.⁶ The equations of motion were integrated by velocity Verlet algorithm with a time step of 1 fs for all simulation runs. The electrostatic interactions were calculated by the Atom Based method with accuracy of 0.001 kcal/mol.

2.2 Force Fields

Force field parameters of oligomer species were based on COMPASS. UiO-66-OH were treated as a rigid framework and the Lennard-Jones parameters were adopted using the universal force field.⁷ Atomic charges for UiO-66-OH were obtained using the Rappe-Goddard charge equilibration method (QEq).⁸ In our calculations, the van der Waals and Coulombic interactions were subject to a 14 Å cutoff.

2.3 Simulation and Analysis Details

2.3.1 Fractional Accessible Volume (FAV) Analysis

The fractional accessible volume (FAV) is the locus of the probe centre as the probe

freely rolls over the framework.⁹ A gas molecule probe is randomly inserted into simulation box and the insertion is considered to be successful if the probe does not overlap with any polymer atom. In the calculation process, N₂ molecule was chosen as the molecule probe. The ratio of successful insertion to the total number of insertion gives FAV. Therefore, it is a reasonable method to determine the changes of free accessible volume. In this study, FAV for constructed cells were obtained using the “connolly surface” from the *Visualizer* module.¹⁰

2.3.2 Grand Canonical Monte Carlo (GCMC) Simulation

The GCMC simulation is a powerful method to analyze the loading-dependent gas adsorption or transport.^{11,12} In this ensemble, temperature T , volume V and chemical potential μ were fixed, while the number of particles N was allowed to be determined. To be specific, the related algorithm generates a series of ‘moves’ that are accepted or rejected according to the following probabilities:

$$P = \exp\left(-\frac{E}{k_B T}\right) \frac{fV_{box}}{(N+1)k_B T} \quad (\text{creation}) \quad (1)$$

$$\text{Probability} = \exp\left(-\frac{E}{k_B T}\right) \frac{Nk_B T}{fV_{box}} \quad (\text{deletion}) \quad (2)$$

$$\text{Probability} = \exp\left(-\frac{E_1 - E_2}{RT}\right) \quad (\text{displacement or rotation}) \quad (3)$$

where E is the potential energy, f is the fugacity, and k_B is the Boltzmann constant.

In present simulation process, the well-known Metropolis algorithm is used to accept or reject a configurational move of gas molecules. The Berendsen thermostat was used for temperature monitoring. 1000000 steps of GCMC calculations were carried out with the initial equilibration period of 100000 steps. To simulate the sorption in the process of gas penetration into porous liquids, tasks of adsorption isotherm and fixed pressure were

performed, respectively. The adsorption density filed distribution of CO₂ in porous liquids were analyzed according to adsorption behavior at 10.0 bar.

3. DATA ANALYSIS



Figure S1. The synthesis of oligomer species of KH560-M2070.

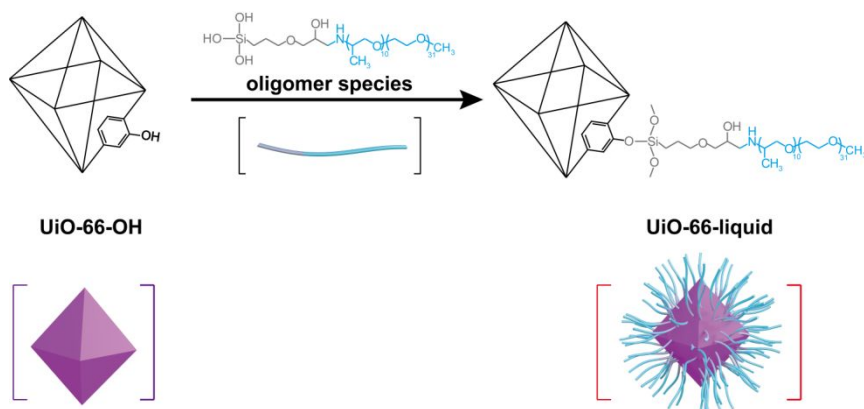


Figure S2. Synthesis of UiO-66-liquid and the illustration of surface changes of UiO-66-OH.

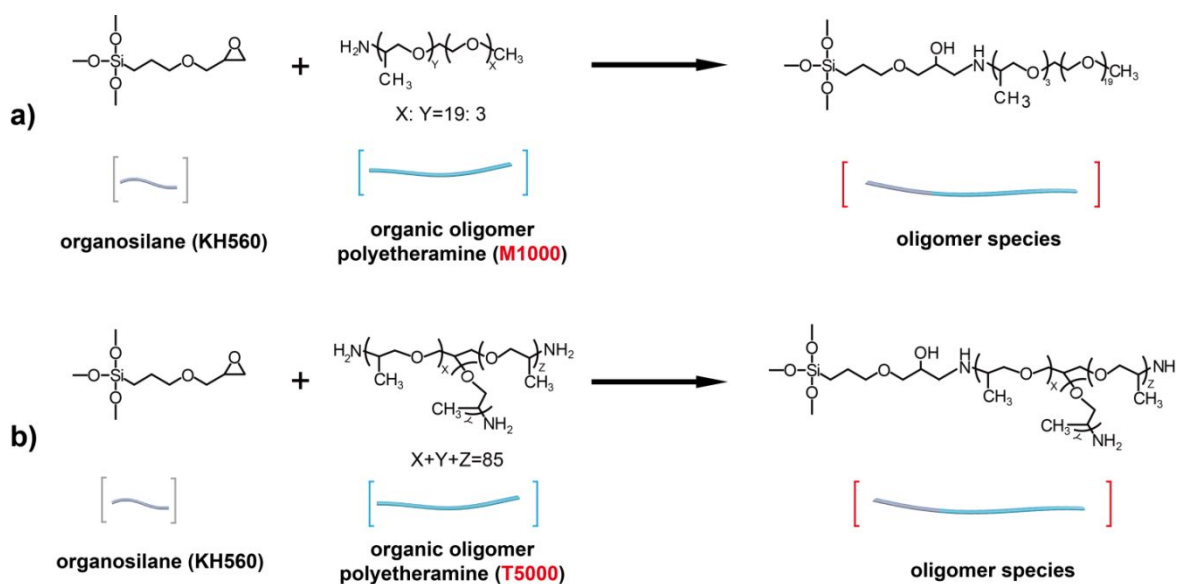


Figure S3. Synthesis of oligomer species of (a) KH560-M1000, and (b) KH560-T5000.

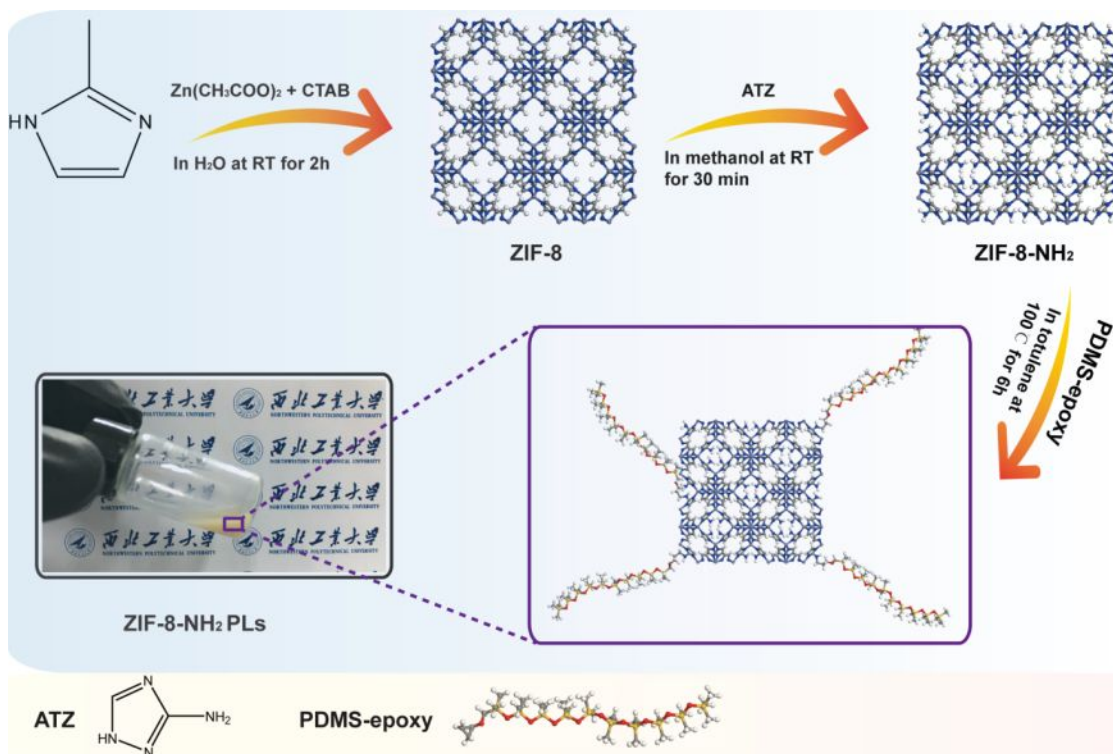


Figure S4. The synthesis of ZIF-8-NH₂ PLs.

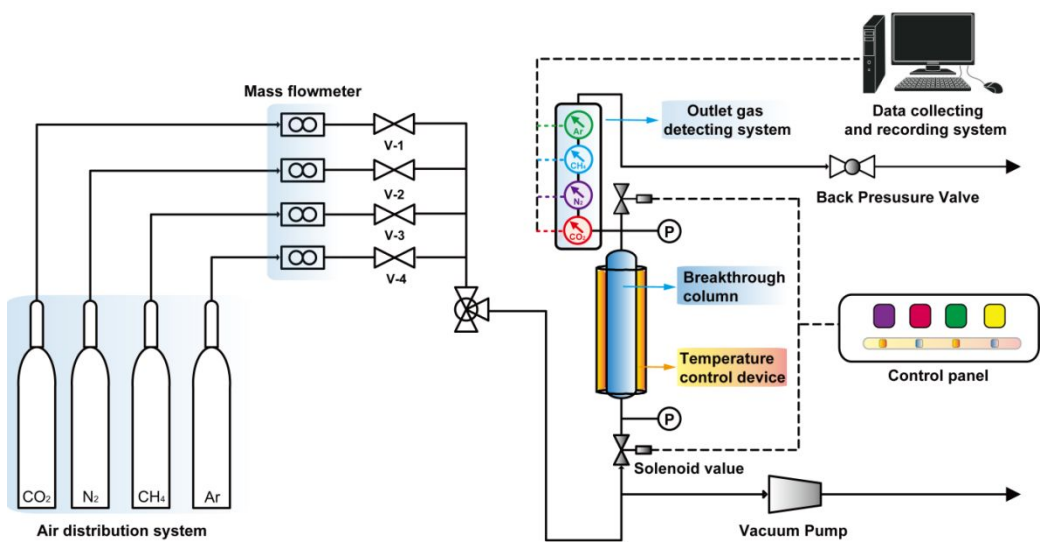


Figure S5. Schematic diagram of installation for breakthrough curve experiments.



Figure S6. The actual pictures of breakthrough curve experiments, (a) The operation panel; (b) The on-line CO₂ detector; (c) Real time control and displaying module.

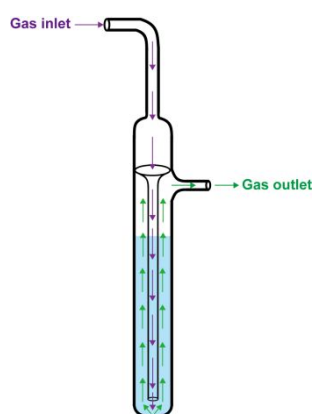


Figure S7. Schematic representation of the breakthrough column loading with PLs.

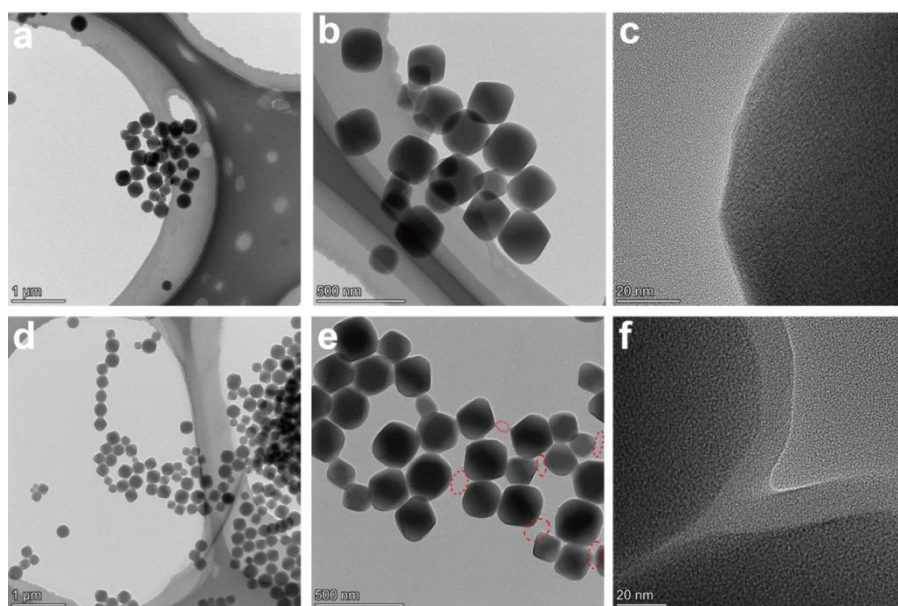


Figure S8. TEM images of UiO-66-OH (a, b, c) and UiO-66-liquid (d, e, f), respectively.

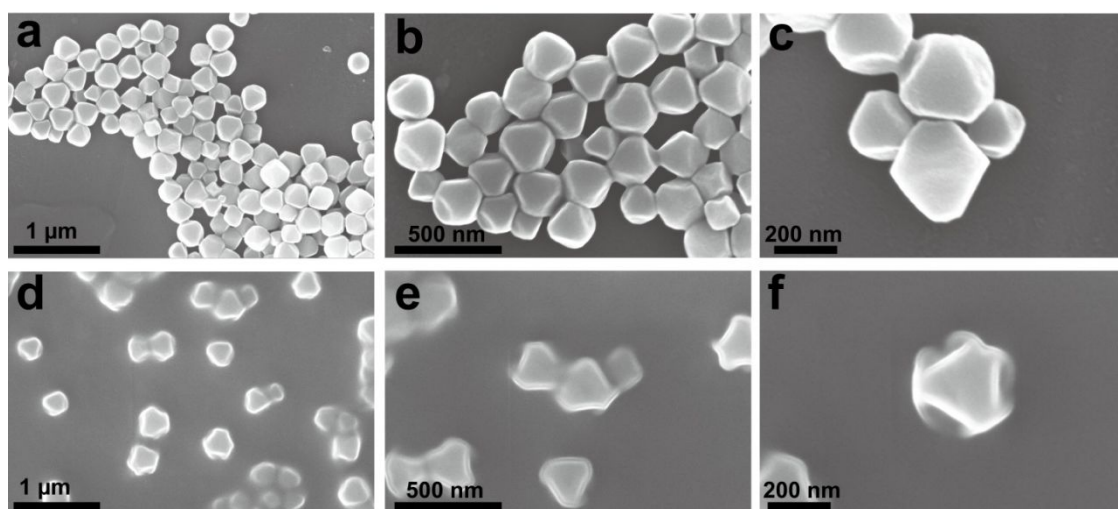


Figure S9. SEM images of UiO-66-OH (a, b, c) and UiO-66-liquid (d, e, f), respectively.

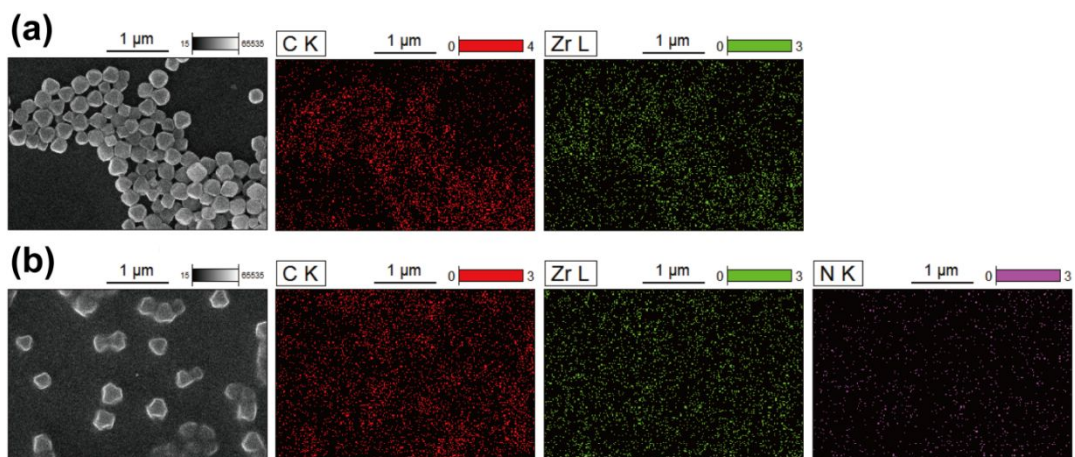


Figure S10. EDS mapping (C, N, Zr) of (a) UiO-66-OH and (b) UiO-66-liquid, respectively.

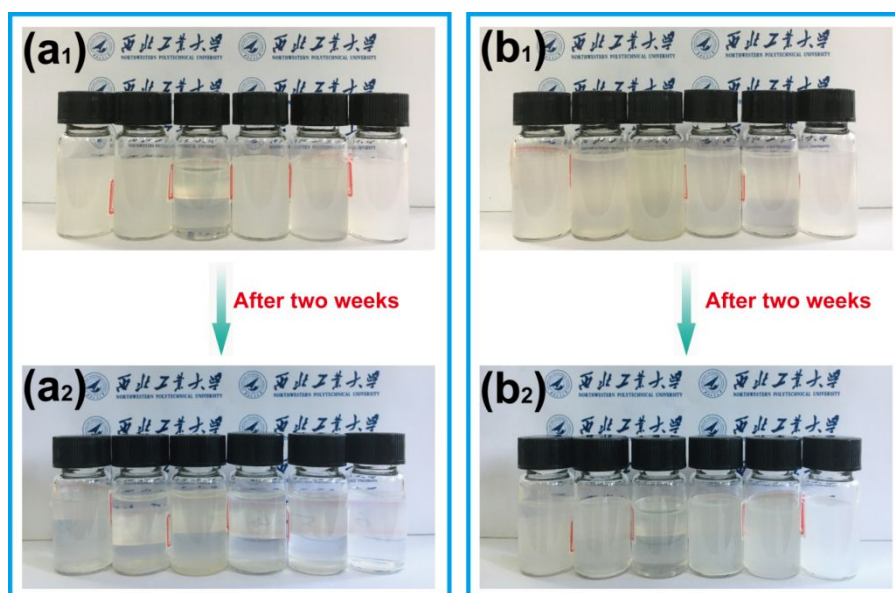


Figure S11. Photos of the pristine UiO-66-OH (a₁) and UiO-66-liquid (b₁) in various common solvents at a concentration of 20 mg·mL⁻¹ as well as after setting for one week (a₂, b₂). The solvents in every photos from left to right are as following: ethanol, DMF, pyridine, chloroform, acetone and tetrahydrofuran (THF).

It can be seen that the agglomeration is serious for pristine UiO-66-OH particles in various solvent after two weeks, while for the UiO-66-liquid, the dispersion ability in most of the above solvents are excellent after two weeks, indicating its good processability in

practical industries.

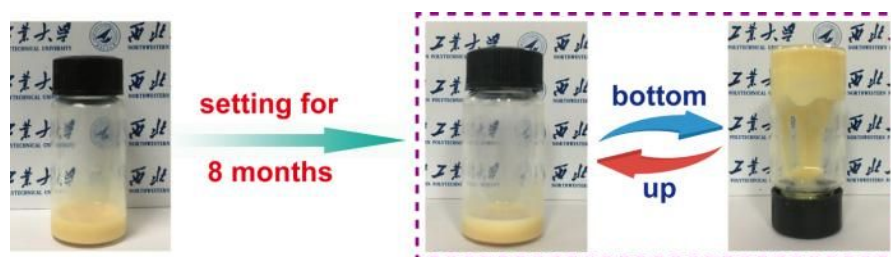


Figure S12. Photos of UiO-66-liquid and the fluidity of UiO-66-liquid after setting for eight months at room temperature.

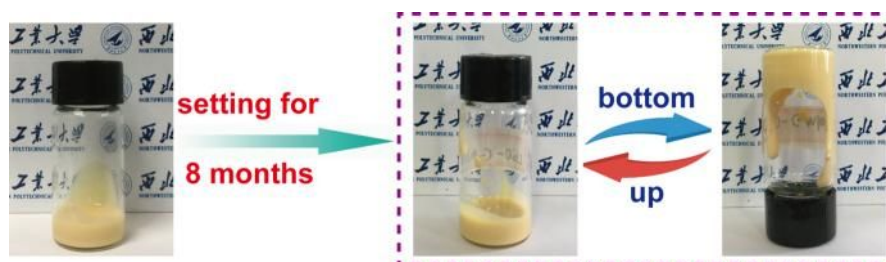


Figure S13. Photos of UiO-66-liquid-M1000.



Figure S14. The photo of UiO-66-liquid-T5000.

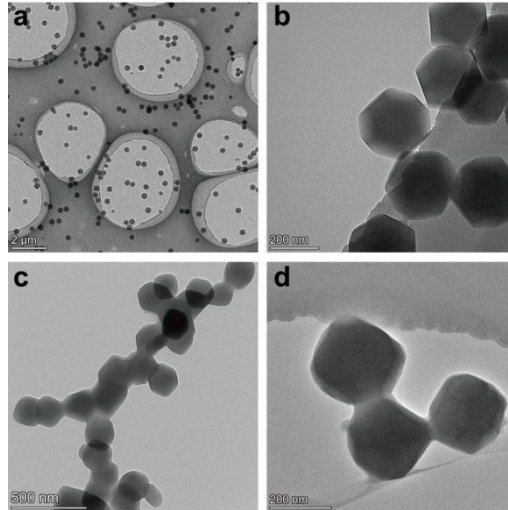


Figure S15. TEM images of ZIF-8-NH₂ (a, b) and ZIF-8-NH₂ PLs (c, d).



Figure S16. Photos of ZIF-8-NH₂ PLs.

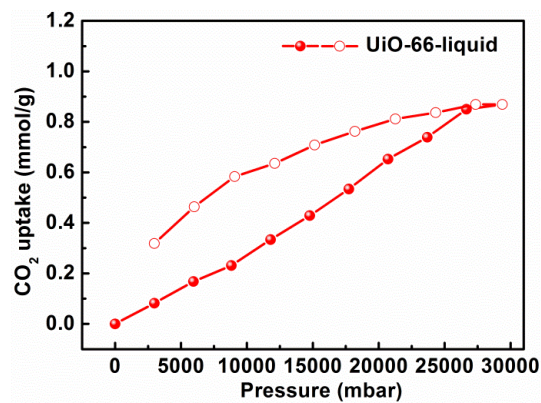


Figure S17. CO₂ adsorption-desorption isotherms of UiO-66-liquid under high pressure (0~30000 mbar) at 25°C. Closed and open symbols represent to adsorption and desorption, respectively.

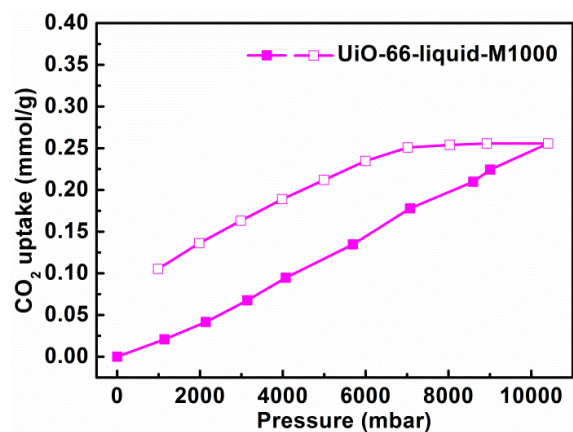


Figure S18. CO₂ adsorption-desorption isotherms of UiO-66-liquid-M1000 under low testing pressure (0~10000 mbar) at 25°C. Closed and open symbols represent to adsorption and desorption, respectively.

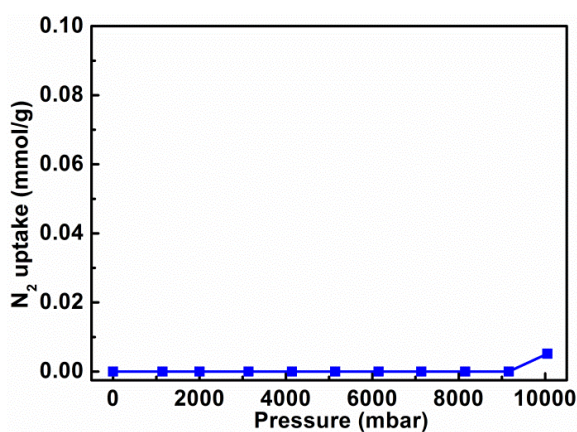


Figure S19. N₂ adsorption isotherms of UiO-66-liquid-M1000 under low testing pressure (0~10000 mbar) at 25°C.

Table S1 Comparison of CO₂ uptake performance between UiO-66 PLs in present study and reported PLs in previous studies.

Sample names	CO ₂ uptake/ (mmol/g)	Testing conditions	Ref.
ZIF-8 PLs	~1.6 mmol/g	298K, 10 bar	13
Hollow silica PLs	0.9 mmol/g	298K, 10 bar	14
15-C-5-PL	0.375 mmol/g	298K, 10 bar	15
18-C-6-PL	0.429 mmol/g	298K, 5 bar	15
Porous aromatic framework PAF-1/Genosorb PLs	0.72 mmol/g	298K, 5 bar	16
Al(fum)(OH)/PDMS PLs	0.95 mmol/g	298K, 5 bar	16
Scrambled cage CC3-R/Hexachloropropene (HCP)	55 μmmol/g	298K, 10 bar	17
UIO-66 PLs	1.66 mmol/g	298K, 10 bar	18
H-ZSM-5 PLs	0.46 mmol/g	298K, 10 bar	19
Porous carbons liquids	0.56 mmol/g	298K, 10 bar	20
UiO-66-liquid	0.86 mmol/g	298K, 30 bar	This study

REFERENCES

- [1] Banerjee R.; Phan A.; Wang B.; Knobler C.; Furukawa H.; O’Keeffe M.; Yaghi O.M. High-Throughput Synthesis of Zeolitic Imidazolate Frameworks and Application to CO₂ Capture. *Science* **2008**, *319*, 939–943.
- [2] Pan Y.; Liu Y.; Zeng G.; Zhao L.; Lai Z.; Rapid Synthesis of Zeolitic Imidazolate Framework-8 (ZIF-8) Nanocrystals in an Aqueous System. *Chem. Commun.* **2011**, *47*, 2071–2073.
- [3] Cho, K. Y.; An, H.; Do, X. H.; Choi, K.; Yoon, H. G.; Jeong, H. K.; Lee, J. S.; Baek, K. Y. Synthesis of Amine-Functionalized ZIF-8 with 3-amino-1,2,4-triazole by Postsynthetic Modification for Efficient CO₂-Selective Adsorbents and Beyond. *J. Mater. Chem. A* **2018**, *6*, 18912–18919 .
- [4] He S.; Chen L.; Cui J.; Yuan B.; Wang H.; Wang F.; Yu Y.; Lee Y.; Li T.; General Way to Construct Micro- and Mesoporous Metal-Organic Framework-Based Porous Liquids. *J. Am. Chem. Soc.* **2019**, *141*, 19708–19714.
- [5] Golzar, K.; Amjad-Iranagh, S.; Amani, M.; Modarress, H. Molecular Simulation Study of Penetrant Gas Transport Properties into the Pure and Nanosized Silica Particles Filled Polysulfone Membranes. *J. Membr. Sci.* **2014**, *451*, 117–134.
- [6] Pazirolf, M.; Dehghani, M.; Niazi, S.; Mohammadi, A.H.; Asghari, M. Molecular Dynamics Simulation and Monte Carlo Study of Transport and Structural Properties of PEBA 1657 and 2533 Membranes Modified by Functionalized POSS-PEG Material, *J. Mol. Liq.* **2017**, *241*, 646–653.
- [7] Rappe, A.K.; Casewit, C.J.; Colwell, K.S.; Goddard, W.A.; Skiff, W.M. UFF, a Full

- Periodic Table Force Field for Molecular Mechanics and Molecular Dynamics Simulations, *J. Am. Chem. Soc.* **1992**, *114*, 10024–10035.
- [8] Rappe, A.K.; Goddard, W.A. Charge Equilibration for Molecular Dynamics Simulations, *J. Phys. Chem.* **1991**, *95*, 3358–3363.
- [9] Akkermans, R.L.C.; Spenley, N.A.; Robertson, S.H. Monte Carlo Methods in Materials Studio, *Molecular Simulation* **2013**, *39*, 1153–1164.
- [10] Connolly, M.L. Computation of Molecular Volume, *J. Am. Chem. Soc.* **1985**, *107*, 1118–1124.
- [11] De Lorenzo, L.; Tocci, E.; Gugliuzza, A.; Drioli, E. Assembly of Nanocomposite PEBAX Membranes: A Complementary Study of Affinity and Clusterization Phenomena. *J. Membr. Sci.* **2012**, *421*, 75–84.
- [12] Bux, H.; Chmelik, C.; Krishna, R.; Caro, J. Ethene/Ethane Separation by the MOF Membrane ZIF-8: Molecular Correlation of Permeation, Adsorption, Diffusion. *J. Membr. Sci.* **2011**, *369*, 284–289.
- [13] Shan, W.; Fulvio, P.F.; Kong, L.; Schott, J.A.; Do-Thanh, C.L.; Tian, T.; Hu, X.; Mahurin, S.M.; Xing, H.; Dai, S. New Class of Type III Porous Liquids: A Promising Platform for Rational Adjustment of Gas Sorption Behavior. *ACS Appl. Mater. Inter.* **2018**, *10*, 32–36.
- [14] Shi, T.; Zheng, Y.; Wang, T.; Li, P.; Wang, Y.; Yao, D.; Effect of Pore Size on the Carbon Dioxide Adsorption Behavior of Porous Liquids Based on Hollow Silica, *Chemphyschem* **2018**, *19*, 130–137.
- [15] Jie, K.; Onishi, N.; Schott, J.A.; Popovs, I.; Jiang, D.E.; Mahurin, S.; Dai, S.

- Transforming Porous Organic Cages into Porous Ionic Liquids *via* a Supramolecular Complexation Strategy. *Angew. Chem., Int. Ed. Engl.* **2020**, *59*, 2268–2272.
- [16] Cahir, J.; Tsang, M.Y.; Lai, B.; Hughes, D.; Alam, M.A.; Jacquemin, J.; Rooney, D.; James, S.L. Type 3 Porous Liquids Based on Non-Ionic Liquid Phases- A Broad and Tailorable Platform of Selective, Fluid Gas Sorbents. *Chem. Sci.* **2020**, 2077–2084.
- [17] Greenaway, R.L.; Holden, D.; Eden, E.G.B.; Stephenson, A.; Yong, C.W.; Bennison, M.J.; Hasell, T.; Briggs, M.E.; James, S.L.; Cooper, A.I. Understanding Gas Capacity, Guest Selectivity, and Diffusion in Porous Liquids. *Chem. Sci.* **2017**, *8*, 2640–2651.
- [18] Zhao, X.; Yuan, Y.; Li, P.; Song, Z.; Ma, C.; Pan, D.; Wu, S.; Ding, T.; Guo, Z.; Wang, N. A Polyether Amine Modified Metal Organic Framework Enhanced the CO₂ Adsorption Capacity of Room Temperature Porous Liquids. *Chem. Commun.* **2019**, *55*, 13179–13182.
- [19] Li, P.; Chen, H.; Schott, J.A.; Li, B.; Zheng, Y.; Mahurin, S.M.; Jiang, D.E.; Cui, G.; Hu, X.; Wang, Y.; Li, L.; Dai, S. Porous Liquid Zeolites: Hydrogen Bonding-Stabilized H-ZSM-5 in Branched Ionic Liquids. *Nanoscale* **2019**, 1515–1519.
- [20] Li, P.; Schott, J.A.; Zhang, J.; Mahurin, S.M.; Sheng, Y.; Qiao, Z.; Hu, X.; Cui, G.; Yao, D.; Brown, S.; Zheng, Y.; Dai, S. Electrostatic-Assisted Liquefaction of Porous Carbons. *Angew. Chem., Int. Ed. Engl.* **2017**, *129*, 15154–15158.